Light-induced orientational effects in periodic photonic structures with pure and dye-doped nematic liquid crystal defects

Andrey E. Miroshnichenko,[1] Etienne Brasselet,[2] and Yuri S. Kivshar[1]
[1]*Nonlinear Physics Centre and Centre for Ultra-high bandwidth Devices for Optical Systems (CUDOS), Australian National University, Canberra ACT 0200, Australia*
[2]*Centre de Physique Optique Moléculaire et Hertzienne, Université Bordeaux 1, CNRS, 351 Cours de la Libération, 33405 Talence Cedex, France*
(Received 22 June 2008; published 19 November 2008)

We theoretically study and compare the light-induced Fréedericksz transition and above-threshold reorientation in pure and dye-doped nematic liquid crystals embedded into periodic dielectric structures. The presence of optical defect modes is found to significantly alter the effective influence of dyes as compared to the standard case of liquid crystal films without periodic structure, which is due to the overall resonant absorption of the dye-doped liquid crystal layer. Both statics and dynamics are discussed. In particular, it is found that optical response time can be up to several orders of magnitude faster with pure liquid crystals than with dye-doped ones. Thermal effects caused by absorption of dyes are also investigated to gauge whether it may induce nematic-to-isotropic phase transition.

DOI: 10.1103/PhysRevA.78.053823 PACS number(s): 42.70.Qs, 42.70.Df, 42.65.Pc

I. INTRODUCTION

The field of photonics has been rapidly growing for the past two decades, showing the possibility of versatile control of light propagation in artificial media. Periodic structures provide an efficient way to spatially route light in various directions exploiting photonic band gaps [1,2], which lead to various phenomena, such as light bending [3], beaming [4], self-collimation [5], and superprism [6] effects. Usually, photonic structures are designed and fabricated in view of specific properties that cannot be changed afterward. An active control of light propagation in these structures is therefore highly desirable. Busch and John [7] originally proposed to benefit from liquid crystals (LCs) sensitivity to external fields using LC infiltration. This approach has been explored in many experimental situations involving thermal [8,9] and electrical [9,10] fields. One of the key issues with regard to smart integrated photonic circuits is to achieve all-optical switching where the propagation properties of the light will be controlled by light itself. Among possible approaches, the most promising one is based on the material nonlinear optical response.

Nematic liquid crystals (NLCs) are particularly interesting materials due to their infiltration capabilities and huge optical nonlinearities associated with molecular ordering [11]. Indeed, the strong coupling between light and NLCs leads to a nonlinear response that is usually several orders of magnitude larger than Kerr nonlinearity in conventional dielectrics. Therefore, easy optical manipulation of NLCs is achieved, with or without a light intensity threshold. In the former case, one deals with the optical Fréedericksz transition (OFT) [12–15] in reference to the first demonstration carried out with quasistatic electric fields [16]. However, the analogy has its limits since light polarization changes due to NLC optical anisotropy are at the origin of a complex spatiotemporal feedback. Such a distinction is well illustrated by the collective molecular rotation in a NLC film under the action of a circularly polarized light [17], which has recently been shown to lead to chaotic rotations using both circular [18] or elliptical [19] intensity profiles.

All-optical devices based on NLC orientational optical nonlinearities have already been achieved to route light by light using solitons [20–23]. In the field of photonic crystals, the discussion of the possible use of LCs for all-optical tunability emerged only recently. One can mention the demonstrations of LCs infiltrated in photonic crystal fibers [24,25] and one-dimensional (1D) [26] or planar [27,28] photonic crystals using absorbing or dye-doped LCs. In these works, the resonant interaction of light induces a change of the order parameter, phase transition, or surface-mediated bulk realignment. In contrast, the use of nonresonant orientational optical nonlinearities has not been explored much. It was shown that the OFT threshold is spectrally modulated within the band gap of a 1D photonic crystal containing a pure NLC layer that generate optical defect modes. In particular, this threshold can be reduced by several orders of magnitude when the pumping light wavelength matches a defect mode frequency [29,30].

In this paper, we study the light-induced Fréedericksz transition and above-threshold orientational effects in one-dimensional dielectric periodic structures with a single defect layer made of pure or dye-doped homeotropically aligned NLC. The latter case is known to exhibit an OFT threshold that could be a few orders of magnitude lower than in the pure case as a result of resonant optical torque enhancement for specific dyes [31], which might be beneficial for possible applications. However, when a dye-doped NLC layer is embedded inside a periodic structure, we show that resonant absorption effects associated with defect modes can become prominent. A systematic comparison of pure and dye-doped behavior under the action of a linearly polarized light field allows us to estimate the overall effect of dye dopants that results from the optical torque enhancement and the effective absorption contributions.

The paper is organized as follows. In Sec. II, we introduce the model that describes the light propagation in a 1D peri-

odic structure containing a single NLC defect layer. Section III gathers results for OFT onset and above-threshold behavior as a function of frequency detuning between pumping light and optical defect modes. Here we explore and discuss both the statics and dynamical aspects of the optical reorientation. In addition, we gauge the role of thermal effects in the dye-doped case, where absorption cannot be neglected in a practical situation. Finally, our conclusions are summarized in Sec. IV.

II. MODEL

The optical Fréedericksz transition for pure NLCs films was first studied within the geometrical optics approximation [15] where the backward-propagating field is neglected and the electric field slowly varying envelope approximation is used. Theoretical results obtained under such assumptions are in good agreement with observations for polarized [32,33], partially polarized [34], or unpolarized [35] light fields. However, these assumptions naturally fail when periodic structures are considered. Indeed, dielectric periodicity is at the origin of so-called photonic band gaps, i.e., a frequency range where light cannot propagate inside the structure, thus leading to total reflection. When periodicity is broken, optical defect modes appear in the band gap. They correspond to well-defined frequencies having total (without absorption) transmission through the structure. These features are the result of interferences between forward- and backward-propagating waves and require the exact solution of Maxwell's equations. Moreover, when periodicity breaking is due to the presence of a reoriented NLC layer, the inhomogeneous spatial profile of the refractive index along the propagation direction affects the light propagation inside the whole periodic structure and implies to solve Maxwell's equations self-consistently [11].

The equations for the director $\mathbf{n}$, which defines the local molecular orientation of the NLC, are obtained in a standard manner using the free-energy density F [11,15],

$$F = F_{\mathrm{el}} + F_{\mathrm{opt}}. \tag{1}$$

The first term is the elastic part that describes all basic deformations of the director field associated with the Frank elastic constants K_n,

$$F_{\mathrm{el}} = \frac{1}{2}[K_1(\nabla \times \mathbf{n})^2 + K_2(\mathbf{n} \times (\nabla \times \mathbf{n}))^2 + K_3|\mathbf{n} \times (\nabla \times \mathbf{n})|^2]. \tag{2}$$

The second term accounts for the light-matter interaction,

$$F_{\mathrm{opt}} = -\frac{1}{16\pi}\mathrm{Re}(\epsilon_{ij})E_i E_j^*, \tag{3}$$

where $\epsilon_{ij} = \epsilon_\perp \delta_{ij} + \epsilon_a n_i n_j$, δ_{ij} is the Kronecker symbol, $\epsilon_a = \epsilon_\parallel - \epsilon_\perp$ determines the optical anisotropy of the NLC, and $\mathrm{Re}(\cdot)$ denotes the real part. The complex dielectric susceptibilities perpendicular ($\perp$) and parallel ($\parallel$) to $\mathbf{n}$ can be written, as long as absorption length is much larger than the wavelength λ, $\epsilon_l = n_l^2 + i n_l \alpha_l / k_0$, where α_l are absorption coefficients, k_0 is the wave number of the incoming wave $k_0 = 2\pi/\lambda$, and $l = \perp, \parallel$ [36]. Note that for pure NLC (i.e., without dye-dopants) we will assume no absorption, $\alpha_\perp = \alpha_\parallel \equiv 0$. In the presence of dye dopants, it is known that the dye molecules give birth to a dye-assisted optical torque usually referred to as the Jánossy effect [31,37–39]. This can be taken into account by introducing the multiplicative factor $[\mathrm{Re}(\epsilon_a) + \eta]/\mathrm{Re}(\epsilon_a)$ to the dielectric torque where η is a phenomenological factor, which can be either positive or negative [40]. A positive η corresponds to dye-enhanced optical torque and is chosen for the present study.

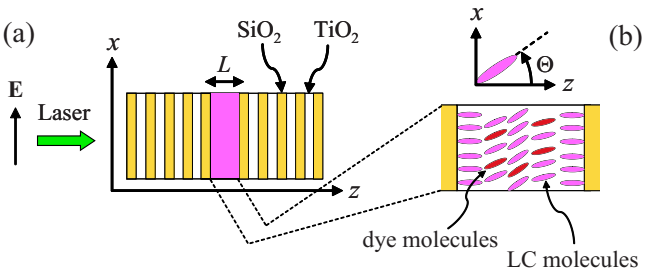

FIG. 1. (Color online) (a) Schematic overview of the one-dimensional periodic structure made of alternating layers of SiO_2 and TiO_2 with a single nematic liquid crystal defect layer of thickness L in its central part. (b) Pure and dye-doped nematic layers are considered; Θ is the director reorientation angle.

For homeotropic alignment and incident plane wave linearly polarized along the x axis, the director can be described by a single angle Θ (see Fig. 1) that only depends on space coordinate z and time t following

$$\mathbf{n}(z,t) = \{\sin\Theta(z,t), 0, \cos\Theta(z,t)\}. \tag{4}$$

The director dynamics is then obtained from Euler-Lagrange equations that take into account the dissipation and is expressed as a partial differential equation,

$$\gamma_1 \frac{\partial\Theta}{\partial t} = -\frac{\delta F}{\delta\Theta}, \tag{5}$$

where γ_1 is the rotational viscosity of the NLC. The homeotropic anchoring boundary conditions $\Theta(0,t) = \Theta(L,t) = 0$ of the NLC layer of thickness L allow to uniquely expand Θ on Fourier basis as

$$\Theta(z,t) = \sum_{m=1}^{\infty} \Theta_m(t)\sin(m\pi z/L), \tag{6}$$

where $\Theta_m(t)$ is the time-dependent amplitude of the mth spatial mode. A set of ordinary differential equations is then obtained from spatial projection onto each mode [32,33],

$$\frac{d\Theta_m}{dt} = 2\int_0^L \frac{\partial\Theta}{\partial t}\sin(m\pi z/L)dz. \tag{7}$$

We found that it is enough to retain the first ten modes, $m = 1, \ldots, 10$, to obtain accurate results within the explored range of incident light intensity.

The light propagation inside the 1D multilayered structure [see Fig. 1(a)] is retrieved using Berreman's 4×4 matrix approach [41] where Maxwell's equations read

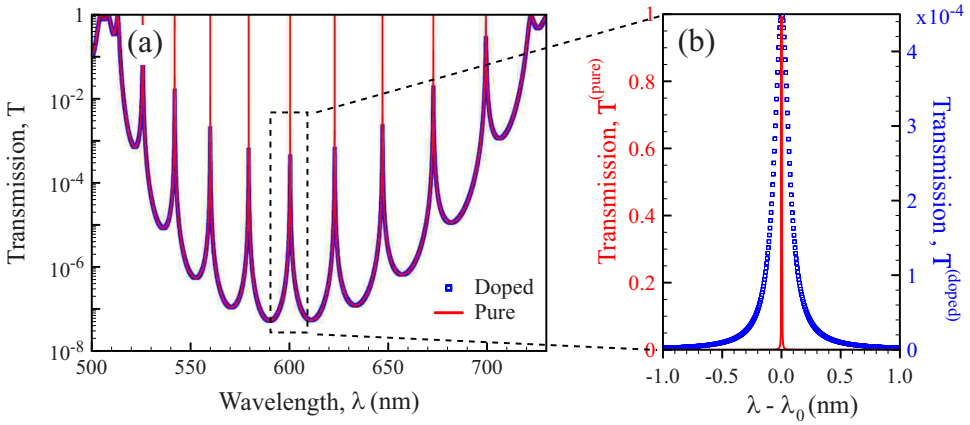

FIG. 2. (Color online) (a) Transmission spectra for pure (red line) and dye-doped (blue squares) LC defects. (b) Zoom around the central defect mode $\lambda_0=599.95$ nm.

$$\frac{d\mathbf{\Psi}}{dz} = ik_0\mathbf{D}(z)\mathbf{\Psi}, \tag{8}$$

with $\mathbf{\Psi}=(E_x,H_y,E_y,-H_x)^T$ and the matrix $\mathbf{D}(z)$ only depends on dielectric properties. Finally, the E_z component of the light field is calculated from the constitutive equation $\nabla\cdot(\epsilon\mathbf{E})=0$, which gives $E_z=-\epsilon_{xz}E_x/\epsilon_{zz}$ [15].

For calculation purposes, the whole structure is divided into thin layers with a constant permittivity tensor that define a finite discrete set of matrices $\mathbf{D}_n$. In the periodic structure on either side of the NLC, the thickness of each layer is that of the actual material, and an adaptive step is used inside the reoriented NLC. The resulting matrix is a product of matrix exponents of all layers, $\mathbf{P}=\Pi_n\exp(ik_0\mathbf{D}_n)$, which links the scattering transmitted ($\mathbf{\Psi}^{(t)}$) amplitude to the incident ($\mathbf{\Psi}^{(i)}$) and reflected ($\mathbf{\Psi}^{(r)}$) ones,

$$\mathbf{\Psi}^{(t)} = \mathbf{P}(\mathbf{\Psi}^{(i)} + \mathbf{\Psi}^{(r)}). \tag{9}$$

For convenience, we introduce normalized intensity $\rho=I/I_{lin}$, where $I_{lin}=\pi^2cK_3\epsilon_\parallel/(\epsilon_a\sqrt{\epsilon_\perp}L^2)$ is the OFT threshold for linearly polarized light [15]. The time t and spatial coordinate z are normalized following $\tau=t/\tau_{NLC}$, with $\tau_{NLC}=\gamma_1L^2/\pi^2K_3$, and $\xi=z/L$. In addition, we define the total phase delay between the extraordinary and ordinary waves with refractive indices $n_e(\xi,\tau)=\{n_\perp^2n_\parallel^2/[n_\parallel^2\cos^2\Theta(\xi,\tau)+n_\perp^2\sin^2\Theta(\xi,\tau)]\}^{1/2}$ and $n_\perp$, respectively,

$$\Delta(\tau) = k_0L\int_0^1 [n_e(\xi,\tau)-n_\perp]d\xi. \tag{10}$$

This integral quantity is a measure of the overall director reorientation, which is accessible to experiments and numerically obtained solving the system $\{d\Theta_m/d\tau\}=0$ [see Eq. (7)] together with Maxwell's equations in a self-consistent manner. For that purpose, we fix the intensity of the light field and use some initial distribution of spatial mode amplitudes $\{\Theta_m^{(0)}\}$. Then, we solve Eq. (9) to find the field distribution inside the NLC and the scattering amplitudes. Inserting the latter light field and initial modes distribution $\{\Theta_m^{(0)}\}$ into the right-hand side of Eq. (7), we calculate its deviation from zero point. Then Newton's method [42] is implemented to find the next set of modes $\{\Theta_m^{(1)}\}$ and the process is iterated until a desired accuracy is reached.

III. RESULTS

We consider a periodic structure made of alternating SiO_2 and TiO_2 dielectric layers [see Fig. 1(a)]. The total number of bilayers from each side is $N=10$. For dielectric layers of thicknesses $d_{SiO_2}=103$ nm and $d_{TiO_2}=64$ nm there is a band gap in the visible range between 520 and 710 nm [43–47]. Without loss of generality, we consider a $L=5$ μm-thick NLC defect layer with typical refractive indices and $n_\parallel=1.7$, $n_\perp=1.5$ and normalized elastic constants $K_1/K_3=2/3$ and $K_2/K_3=1/2$. For the dye-doped case, we consider a mixture of 5CB (4′-*n*-pentyl-4-cyanobiphenyl) nematic doped with 0.1% wt. of AD1 dye for which $\alpha_\perp=42$ cm^{-1}, $\alpha_\parallel=190$ cm^{-1}, and $\eta=58$ [48].

A. Optical properties of the photonic structure with a nematic defect layer

The transmission spectra $T(\lambda)$ for pure and dye-doped cases below OFT are shown in Fig. 2, where $T=|E_x^{(t)}|^2/|E_x^{(i)}|^2$. As a result of absorption, the closer a defect mode is to the center of the band gap, the smaller is the transmission peak and the larger is the full width at half-height, $\Delta\lambda$. As an example, the spectral width of the central defect mode located at $\lambda=\lambda_0=599.95$ nm is $\Delta\lambda_0^{(pure)}=0.01$ nm for pure NLC while $\Delta\lambda_0^{(doped)}=0.2$ nm in the dye-doped case [see Fig. 2(b)].

Figure 3 reveals the typical spatial structure of the defect modes in the pure and dye-doped cases. In the former case, we observe the expected exponential decay of the intensity profile envelope into the periodic structure [see Fig. 3(a)], while in the latter case some light is localized at the edges of the structure as well [see Fig. 3(b)]. However, the electric field profiles inside the NLC layer, and its neighborhood, are identical in both cases [see Figs. 3(c) and 3(d)], as expected from the fact that the light field in the defect layer is only governed by the surrounding periodic structures.

Above OFT threshold the effective refractive index n_e experienced by light becomes z-dependent and its amplitude

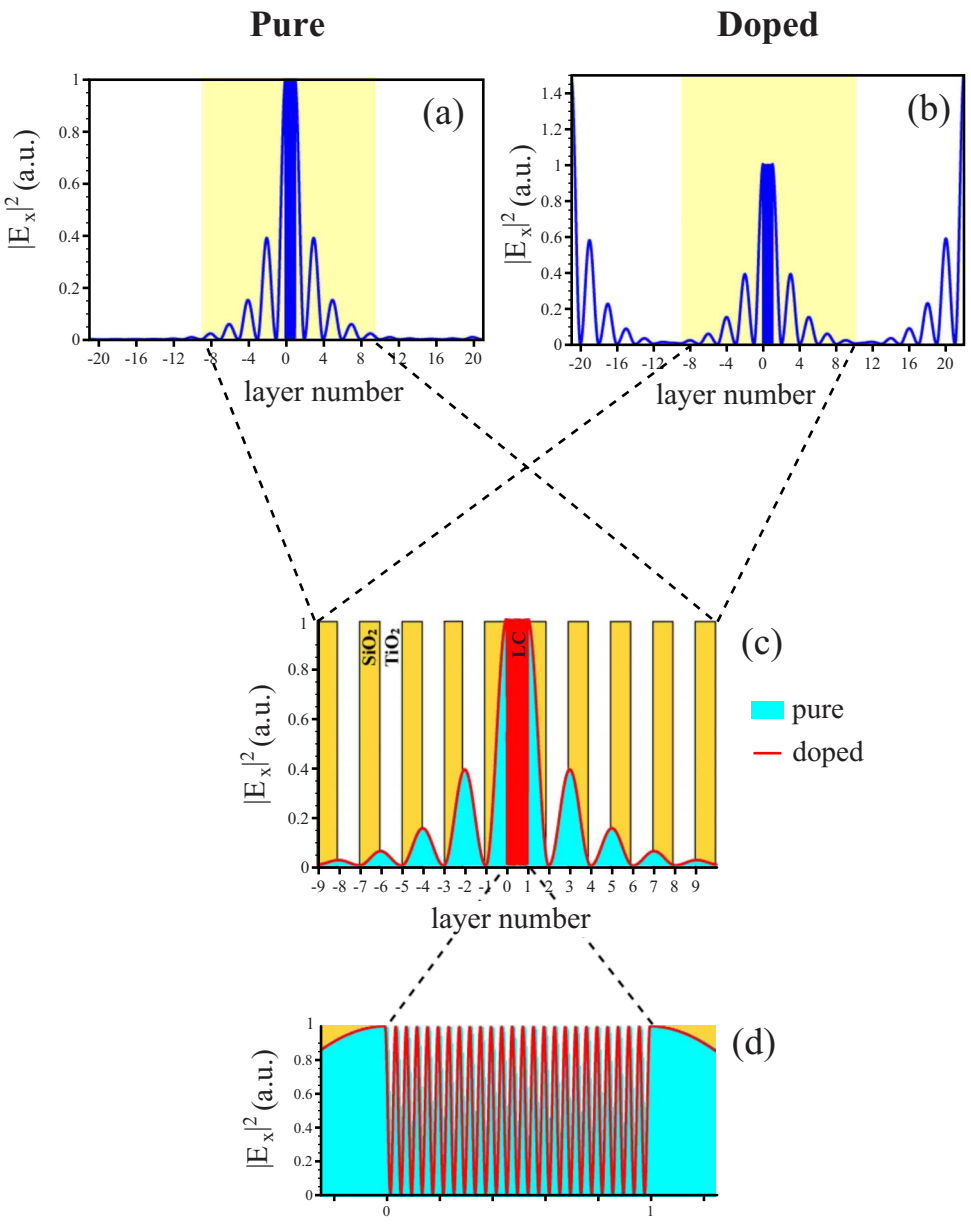

FIG. 3. (Color online) Normalized electric field intensity (taking arbitrarily max $|E_x|^2=1$ inside the NLC layer) of the electric field at the central defect mode frequency ($\lambda=\lambda_0$) for pure (a) and (b) dye-doped cases; (c) superimposed light field intensities of pure (filled area) and dye-doped (red line) NLC from shadowed areas in (a) and (b); (d) defect mode profile enlargement inside the NLC layer exhibiting standing waves that result from interferences between forward- and backward-propagating waves. The defect mode has a similar profile in the central part of the structure in both cases.

increases with Θ for present homeotropic geometry. This leads to a redshift of the defect mode frequency comb, whose maximum value is typically $\lambda_0(n_\parallel-n_\perp)/n_\perp \approx 80$ nm. In this work, the maximal redshift is about 30 nm.

B. Spectrally modulated Fréedericksz transition threshold

Figure 4 shows the dependence of the normalized OFT threshold, ρ_{th}, versus pumping wavelength. Numerically, ρ_{th} is calculated from linear stability analysis of the fixed point that corresponds to $\Theta \equiv 0$. The threshold is found to be spectrally modulated in both situations. The presence of dyes implies an amplification of the optical torque by a factor $\zeta=[\text{Re}(\epsilon_a)+\eta]/\text{Re}(\epsilon_a)\approx 100$ as compared to the pure case resulting in a threshold lowering by a factor ζ in single slab geometry [31]. However, the ratio

$$r_{\text{th}} = \frac{\rho_{\text{th}}^{(\text{pure})}}{\rho_{\text{th}}^{(\text{doped})}} \tag{11}$$

is wavelength-dependent. Indeed, $r_{\text{th}} \approx 100$ in between two defect mode frequencies [see Fig. 5(a)], whereas $r_{\text{th}} \ll 100$ in the vicinity of each defect mode. Moreover, this ratio can be much smaller than 1, $r_{\text{th}} \ll 1$ [see Fig. 5(a)].

These observations can be explained recalling that absorption is present in the dye-doped case, which leads to a

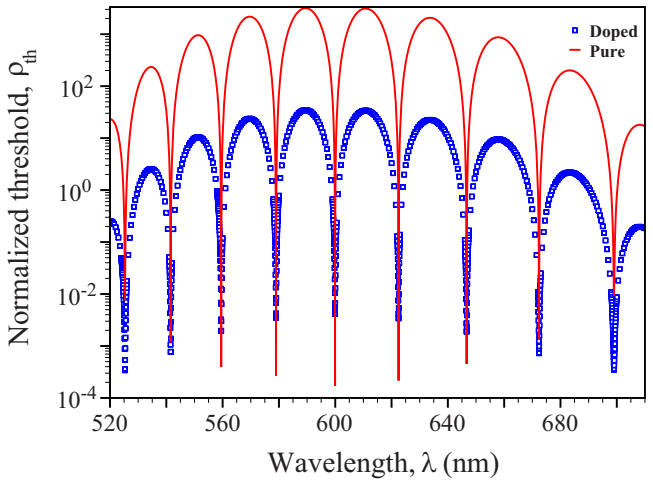

FIG. 4. (Color online) OFT normalized threshold intensity for pure (red line) and dye-doped (blue squares) cases inside the band gap vs pumping light wavelength.

decrease of the effective optical torque. In fact, resonant absorption at defect modes can be sufficiently important to overcome the contribution of dye-enhanced optical torque. Such a competition between absorption and torque enhancement can be seen in Fig. 5(a), where $r_{th}<1$ for some frequencies in the middle of the band gap and $r_{th}>1$ near the edges.

More quantitatively, the OFT threshold is inversely proportional to the averaged light intensity inside the NLC layer. Therefore, one may expect $\rho_{th}\propto 1/\langle|E_x|^2\rangle$, where $\langle\cdots\rangle$ means spatial averaging over the NLC defect slab taking $\Theta\equiv 0$, which implies the following relationship:

$$r_{th}=\zeta\frac{\langle|E_x^{(\mathrm{doped})}|^2\rangle}{\langle|E_x^{(\mathrm{pure})}|^2\rangle}, \tag{12}$$

where the factor ζ explicitly accounts for dye enhancement of the optical torque. In between defect mode frequencies there is poor field localization inside the NLC layer. Consequently, recalling that the absorption length $1/\alpha_\perp \approx 200\ \mu$m is much larger than the thickness of the NLC layer, $L=5\ \mu$m in our case, we get $\langle|E_x^{(\mathrm{doped})}|^2\rangle\sim\langle|E_x^{(\mathrm{pure})}|^2\rangle$, namely $r_{th}\simeq\zeta$ according to Eq. (12) [see Fig. 5(b)]. In contrast, there is resonant absorption near defect mode frequencies due to efficient field localization. In such cases, $\langle|E_x^{(\mathrm{pure})}|^2\rangle\gg\langle|E_x^{(\mathrm{doped})}|^2\rangle$ for the same incident field, which may result in $r_{th}\ll 1$ in the central region of the band gap (see Fig. 5).

We notice that the situations $r_{th}>1$ and $r_{th}<1$ correspond to an effective dye-doped NLC film (without periodic struture) having a positive and negative, respectively, effective coefficient η_{eff}, which is defined as $\eta_{\mathrm{eff}}=\epsilon_a(r_{th}-1)$ and ranges on the interval $[-\epsilon_a,\eta]$. In general, a negative η signifies that the dye-induced contribution to the total torque is of opposite sign with respect to the nonresonant dielectric optical contribution. The observation of positive or negative η for a given pair of NLC and dye compound in films was reported early when the excitation wavelength is varied within the dye absorption linewidth [49]. Here, where a dye-doped NLC layer with $\eta>0$ is embedded inside a periodic structure, η_{eff} changes its sign but keeping $\eta>0$. Indeed, such a change occurs on a typical linewidth of a defect mode, which is several orders of magnitude lower than the absorption linewidth of a dye molecule.

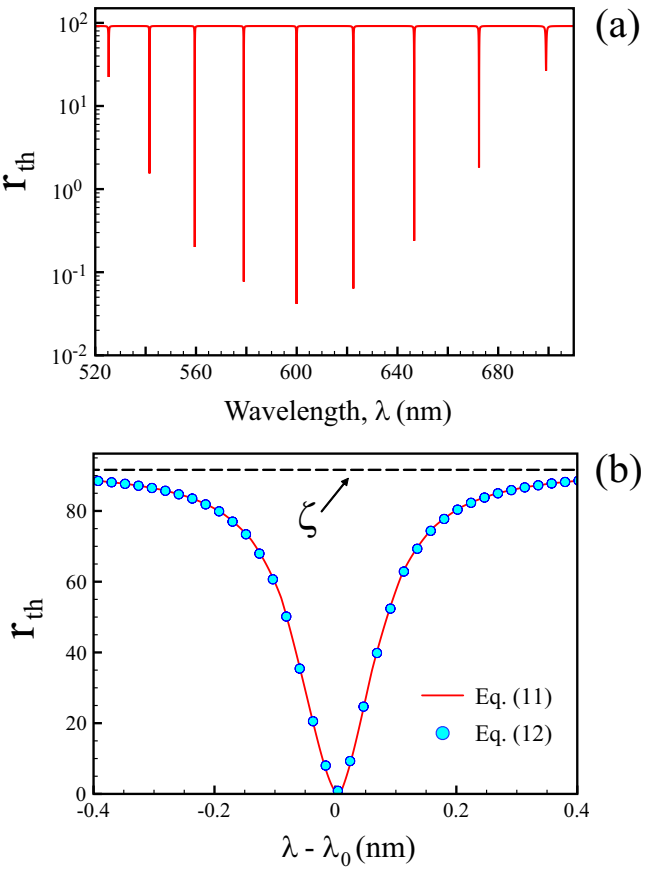

FIG. 5. (Color online) (a) Ratio between normalized OFT threshold intensities for pure and dye-doped cases, following Eq. (11) (b) Zoom around the central defect mode at $\lambda=\lambda_0$ (red line) with the superimposed solution obtained from Eq. (12) (blue circles). The dashed line corresponds to the amplification factor ζ.

C. Reorientation diagrams

As shown in Ref. [30], the order of the Fréedericksz transition depends on the detuning between the pumping wavelength λ_p and nearest defect mode wavelength $\lambda_d(\Theta=0)$ in the absence of reorientation, $\delta_0=\lambda_p-\lambda_d(\Theta=0)$ (see Fig. 6). Note that according to Fig. 4 the threshold power $\rho_{th}(\lambda)$ has local minima at $\lambda=\lambda_d(\Theta=0)$. For positive detuning ($\delta_0>0$) the OFT is first-order and accompanied with orientational hysteresis. This originates from the redshift experienced by the defect mode frequencies when $\Theta\neq 0$. Indeed, just above the threshold, let us consider an infinitesimal nonzero orientational fluctuation $\Theta\ll 1$. The latter corresponds to a decrease of the effective detuning with respect to its original value, $0<\delta(\Theta)<\delta_0$ [see Fig. 6(a)], for which the light field is better localized inside the NLC layer and the optical torque is consequently higher. As a result of such a positive feedback mechanism the fluctuation amplitude increases un-

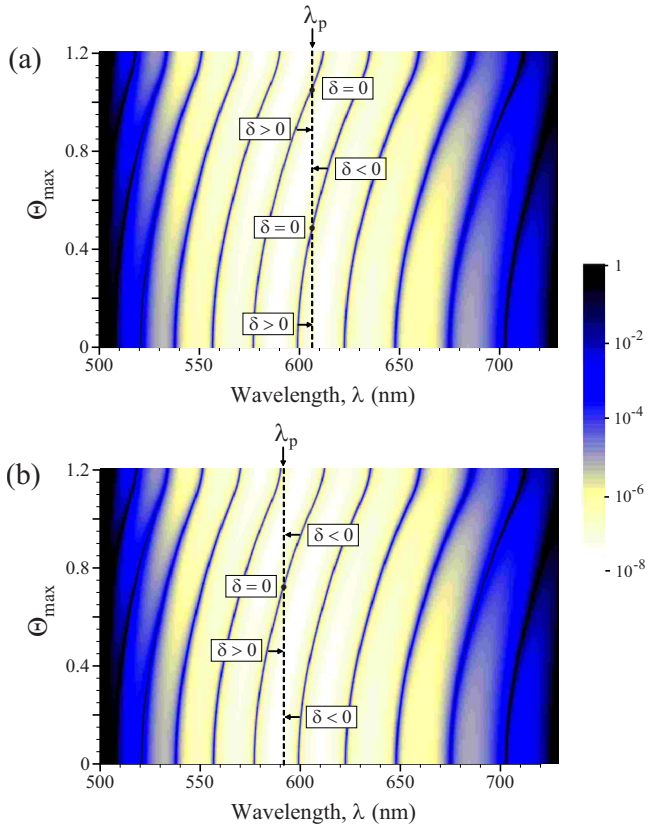

FIG. 6. (Color online) Variation of the linear transmission spectrum vs maximum reorientation angle Θ_{max} in the case of a pure NLC defect for $\delta_0>0$ (a) and $\delta_0<0$ (b), where δ_0 is the difference between of the pumping wavelength λ_p and the nearest defect mode in the absence of reorientation ($\Theta=0$). Calculation is done using the actual stationary angle distribution $\Theta(z)$. Dashed lines illustrate positive and negative detuning with respect to $\lambda=\lambda_0$. Colorscaling from white to black corresponds to increasing transmission. The Θ dependence of the effective detuning δ is illustrated in both panels (a) and (b) for positive, negative, and null situations.

til the effective detuning becomes negative, $\delta(\Theta)<0$ [see Fig. 6(a)]. Then, an equilibrium situation settles where the restoring elastic torque is balanced by the overall optical torque.

For negative detuning, $\delta_0<0$, there is no positive feedback mechanism at threshold. This is due to the fact that the nearest mode moves away from the pumping frequency ($|\delta(\Theta)|>\delta_0$ [see Fig. 6(b)]), which in turn prevents the optical torque from being enhanced.

Reorientation diagrams $\Delta(\rho)$ are shown in Fig. 7, which illustrates the above-mentioned generic behavior for both pure and dye-doped cases for different values of the detuning parameter, $\delta_0=0$, ±0.05, and ±0.5 nm. Above the threshold ρ_{th}, secondary instabilities are predicted for both positive and negative detuning. These bifurcations are associated with a multistable orientational behavior, and their appearance can be understood following previous reasoning about effective detuning $\delta(\Theta)$. Indeed, a positive feedback mechanism appears each time $\delta(\Theta)$ change its sign (see Fig. 6). Such a multistability can be achieved for any wavelength inside the band gap for high enough intensity. In addition, we note the almost 100% hysteresis width due to drastic OFT threshold lowering at defect mode frequencies, $\rho_{th}(\lambda_d)\ll1$.

D. Switching dynamics

Besides stationary solutions, reorientation dynamics may be retrieved from Eqs. (7) and (8). For linearly polarized pumping light, a dynamical behavior is only associated with transients since any orientational state always converges toward a fixed point under a constant incident intensity. Figure 8 presents the switching dynamics for the pure and doped cases, which are obtained by fixing the incident intensity above the OFT threshold value for a detuning parameter $\delta_0=\pm0.5$ nm and taking a nonzero initial distribution for mode amplitudes that mimics a thermal fluctuation. In practice, we set all Θ_m to zero except $\Theta_1=0.01$. Switching dynamics of both the phase delay and transmission are plotted in Fig. 8. In this figure, the intensity is fixed above the OFT threshold value, $\rho_0>\rho_{th}$ (see Fig. 7). In the pure case, we choose $\rho_0^{(pure)}=5000$. That may sound anomalously high, however one must recall that it refers to the incident intensity onto the structure where nonzero detuning is associated with strong reflections. Similarly, we choose $\rho_0^{(doped)}=80$ in the dye-doped case.

The dynamics of the phase delay, although monotonous, shows plateaulike behavior reminiscent of the multistable character of the stationary reorientation diagrams (see Fig. 7). As expected, these plateaux correspond to almost constant transmission, however, transmission spikes are observed in between. The latter are related to a transient fast-growing phase delay (see Fig. 8). Each of these spikes is the optical signature of a dynamical resonance where one defect mode frequency matches the pumping wavelength $\delta(\Theta)=0$. These features are independent of the initial detuning sign and the presence or not of dyes, nevertheless there are quantitative differences. First, the second-order transition for $\delta_0<0$ is associated with a transmission decrease at the early stage of the dynamics, which indicates that the closest defect mode is moving away from the pumping wavelength, while the first-order transition for $\delta_0>0$ montonously leads to a transmission peak. Second, the transmission maxima are very small in the dye-doped case while there is full transmission for pure NLC, $\max[T^{(doped)}]\ll\max[T^{(pure)}]=1$, which is merely due to resonant absorption when $\delta(\Theta)=0$. Finally, the full width at half-height of these dynamical resonances can be extremely small as compared to the characteristic reorientation time of the NLC. Indeed, the transmission linewidth is $\Delta\tau^{(pure)}\sim10^{-10}$ in the pure case [see Figs. 8(a) and 8(b)] while it is $\Delta\tau^{(doped)}\sim10^{-5}$ in the dye-doped case [see Figs. 8(c) and 8(d)].

Such ultrafast optical response times result from the conjunction of narrow defect mode spectral widths of the actual structure (see Sec. III A) with the transient positive feedback mechanism discussed in Sec. III C. In the presence of absorption, we learned that the defect modes linewidth satisfies $\Delta\lambda_0^{(doped)}/\Delta\lambda_0^{(pure)}=20$ [see Fig. 2(b)], which cannot explain the observed ratio $\Delta\tau^{(doped)}/\Delta\tau^{(pure)}\sim10^5$. In fact, this huge ratio is explained from a less efficient positive feedback mechanism due to resonant absorption that drastically re-

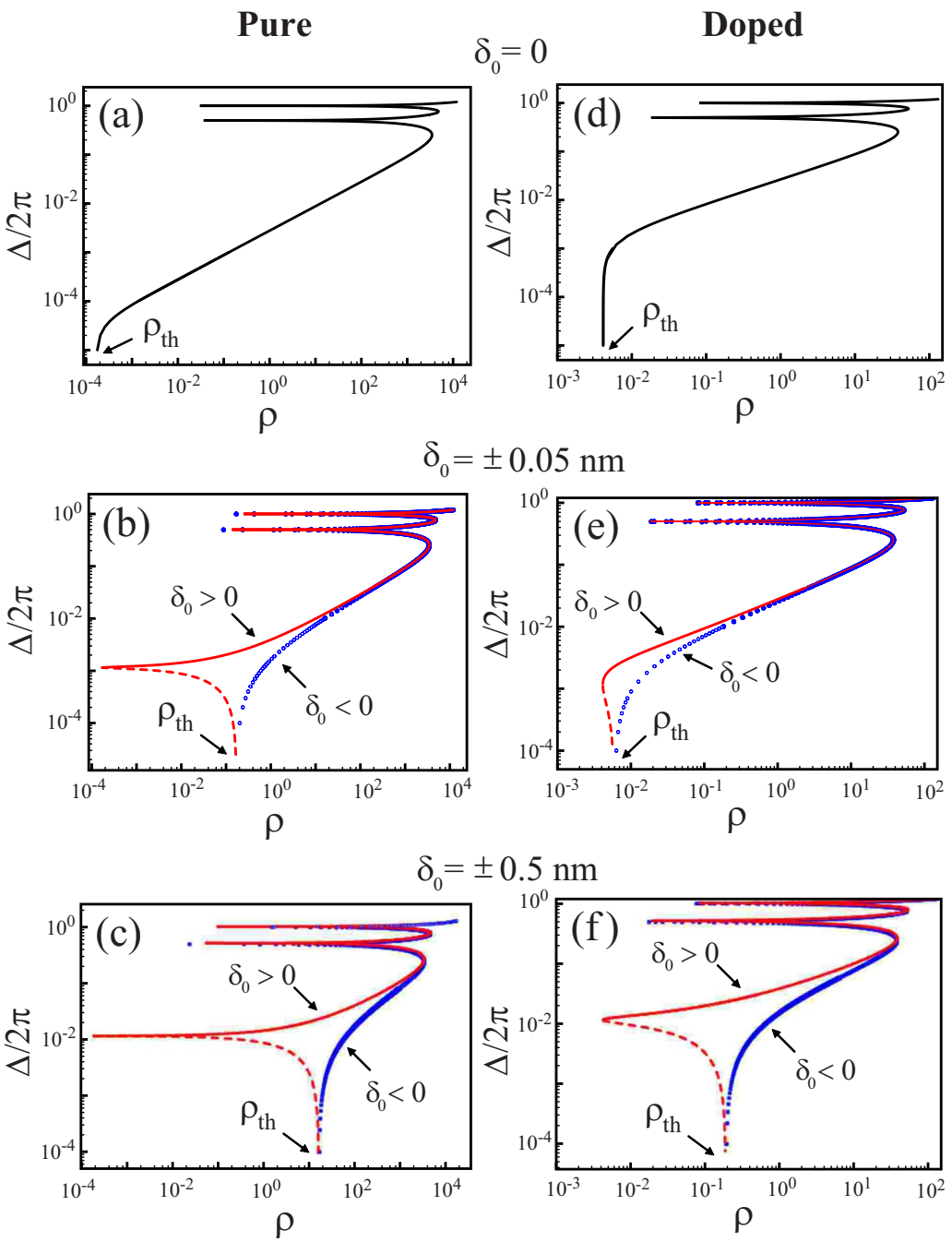

FIG. 7. (Color online) Static reorientation diagrams $\Delta/2\pi$ vs ρ for pure (a), (b), (c) and dye-doped (d), (e), (f) cases for different detuning values: δ_0=0 (a), (d); ±0.05 nm (b), (e); and ±0.5 nm (c), (f), where δ_0 corresponds to the frequency difference between the pumping light and the defect mode at λ_0=599.95 nm.

duces the effective optical torque exerted onto the director.

Recalling that the response time is $\tau_{NLC} \approx 25$ ms of the present 5-μm-thick layer, we obtain optical transmission pulses of the order of picoseconds in the pure case and hundreds of nanoseconds in the dye-doped case.

E. Thermal effects

In previous sections, the nematic liquid crystal heating due to laser absorption in the dye-doped case has not been taken into account. It is worthwhile to gauge whether the temperature variation lies within the range that corresponds to the nematic phase. We propose a simplified heating model that allows us to estimate the temperature elevation as a function of the absorbed fraction of incident light. For this purpose, we assume an incident Gaussian light beam focused onto the NLC layer of thickness L with beam waist w_0 at e^{-2} of the maximum intensity. Moreover, if the Rayleigh range of the Gaussian beam, $2\pi w_0^2/\lambda$, is larger than L, the intensity cross-section profile within the NLC layer can be assumed z independent and the incident intensity profile is written $I_{inc} = I_0 \exp(-2r^2/w_0^2)$, where $r=(x^2+y^2)^{1/2}$. For L=5 μm, the

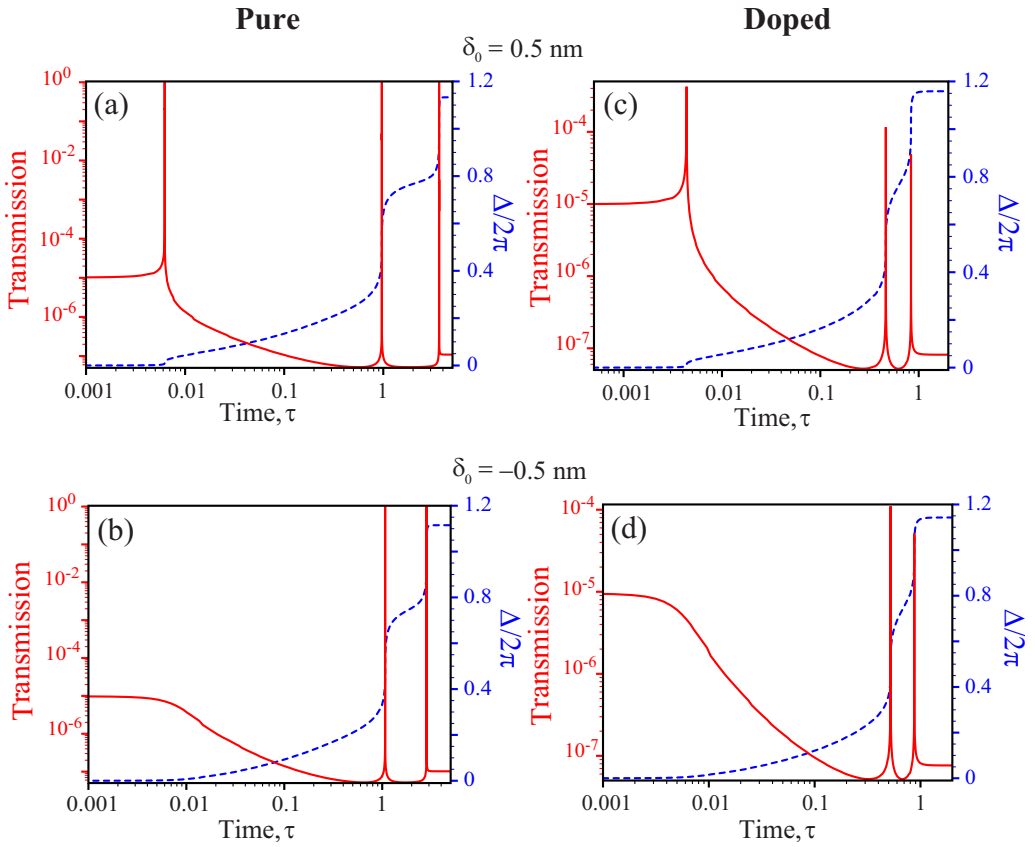

FIG. 8. (Color online) Dynamics of the reorientation for pure (a), (b) and dye-doped (c), (d) cases for δ_0=0.5 nm (a), (c) and δ_0 =−0.5 nm (b), (d) detuning. See text for details. Solid lines (red) represent transmission and dashed lines (blue) refer to the phase delay $\Delta/2\pi$.

later condition is safely fulfilled down to w_0=1 μm. Finally, noting that a real structure would typically correspond to a liquid-crystal layer embedded into 1-mm-thick glass substrates (on which the dielectric multilayers are deposited, whose total thickness is much smaller), we will consider the limiting case of semi-infinite nonabsorbing substrates. In that case, the heating problem can be solved exactly following the approach of Lax [50]. The corresponding geometry is illustrated in Fig. 9(a).

Let us first solve the stationary problem, where the temperature field $T(r,z)$ is a solution of

$$\kappa_\perp\left(\frac{\partial^2 T}{\partial r^2}+\frac{1}{r}\frac{\partial T}{\partial r}\right)+\kappa_\parallel\frac{\partial^2 T}{\partial z^2}=-\alpha I \tag{13}$$

for $0<z<L$ and

$$\kappa_S\left(\frac{\partial^2 T}{\partial r^2}+\frac{1}{r}\frac{\partial T}{\partial r}+\frac{\partial^2 T}{\partial z^2}\right)=0 \tag{14}$$

for $z<0$ and $z>L$, where $\kappa_\perp$, $\kappa_\parallel$, and κ_S are the thermal conductivities of the nematic liquid crystal and the substrate, respectively. In the heat source term, $\alpha(r,z)$ and $I(r,z)$ are the local linear absorption and light intensity. Knowledge of the latter function in the heat source term requires a solution of the full three-dimensional problem of the light-induced NLC reorientation inside a 1D periodic structure. However, for estimation purposes we will further use the 1D plane-

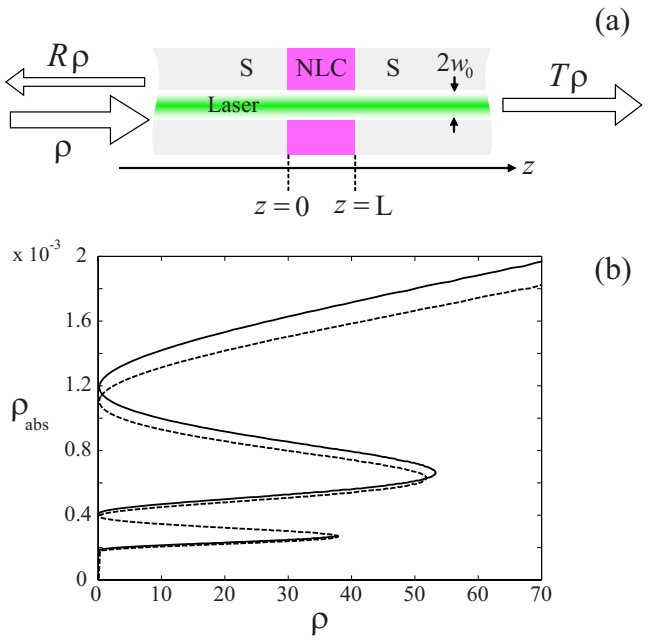

FIG. 9. (Color online) (a) Cylindrically symmetric geometry of the simplified heating problem and definition of normalized absorbed intensity ρ_{abs}. S, glass substrate; NLC, nematic liquid crystal. Calculated dependence of the absorption ρ_{abs} vs input power ρ in the static regime [see Fig. 7(f)] for δ_0=0.5 nm (solid line) and δ_0=−0.5 nm.

wave calculations presented so far to get a typical director profile. Since typically we have $\alpha L \ll 1$ for $L=5$ μm, we get $\alpha I \simeq \alpha I_0 \exp(-2r^2/w_0^2)$ to the first order in α, and noting that $\alpha I_0 \simeq (I_0 - I_0 e^{-\alpha L})/L$, we introduce the absorbed intensity at $r=0$, $I_{\mathrm{abs}}=\alpha I_0 L$. In connection with previous sections, I_{abs} can be related to the normalized absorbed intensity ρ_{abs} following $I_{\mathrm{abs}}=\rho_{\mathrm{abs}} I_{\mathrm{lin}}(w_0)$, where $I_{\mathrm{lin}}(w_0)$ is the OFT intensity threshold in the case of finite beam size, for which a reasonable approximated analytical expression is $I_{\mathrm{lin}}(w_0)=I_{\mathrm{lin}}[1+L\sqrt{2}/(\pi w_0)]^2$ [51]. The value of ρ_{abs} is obtained from the relation $\rho_{\mathrm{abs}}=\rho(1-R-T)$, where R and T are the reflection and transmission coefficients of the whole structure as illustrated in Fig. 9(a).

Then, neglecting the anisotropy of the NLC thermal conductivity tensor, we will further retain a single typical value κ_{LC}, and the original problem given by Eqs. (13) and (14) is cast in the form

$$\frac{\partial^2 T}{\partial r^2} + \frac{1}{r}\frac{\partial T}{\partial r} + \frac{\partial^2 T}{\partial z^2} = -\frac{\rho_{\mathrm{abs}} I_{\mathrm{lin}}(w_0)}{\kappa_{\mathrm{LC}} L} e^{-2r^2/w_0^2}, \tag{15}$$

$$\frac{\partial^2 T}{\partial r^2} + \frac{1}{r}\frac{\partial T}{\partial r} + \frac{\partial^2 T}{\partial z^2} = 0 \tag{16}$$

in the liquid crystal and the substrate, respectively. These equations are associated with boundary conditions for temperature and heat flux at the interfaces between liquid crystal and substrates,

$$T(z=0^+,L^-) = T(z=0^-,L^+),$$

$$\kappa_{\mathrm{LC}}\frac{\partial T}{\partial z}(z=0^+,L^-) = \kappa_{\mathrm{S}}\frac{\partial T}{\partial z}(z=0^-,L^+). \tag{17}$$

Next, the problem is solved applying the Hankel transform $\int_0^\infty r J_0(kr)[\cdots]dr$ to Eqs. (15) and (16), where J_0 is the Bessel function of the first kind. We obtain

$$\frac{\partial^2 \tilde{T}}{\partial z^2} - k^2 \tilde{T} = -\frac{\rho_{\mathrm{abs}} I_{\mathrm{lin}}(w_0) w_0^2}{4\kappa_{\mathrm{LC}} L} e^{-k^2 w_0^2/8}, \tag{18}$$

$$\frac{\partial^2 \tilde{T}}{\partial z^2} - k^2 \tilde{T} = 0 \tag{19}$$

for the liquid crystal and the substrate, respectively, where $\tilde{T}(k,z)=\int_0^\infty r T(r,z) J_0(kr) dr$. For the liquid crystal, the solution is obtained straightforwardly as

$$\tilde{T}(k,z) = \frac{\rho_{\mathrm{abs}} I_{\mathrm{lin}}(w_0) w_0^2}{4k^2 \kappa_{\mathrm{LC}} L} e^{-k^2 w_0^2/8}(1 + F_+ e^{kz} + F_- e^{-kz}), \tag{20}$$

where the functions $F_\pm(k)$ are obtained from boundary conditions as

$$F_\pm(k) = \frac{\mp(1 \pm \kappa) \pm (1 \mp \kappa) e^{\mp kL}}{(1+\kappa)^2 e^{kL} - (1-\kappa)^2 e^{-kL}}, \tag{21}$$

where $\kappa = \kappa_{\mathrm{LC}}/\kappa_{\mathrm{S}}$. Finally, the elevation temperature $dT(r,z)$ is obtained from $\tilde{T}(k,z)$ as $dT(r,z)=\int_0^\infty k\tilde{T}(k,z) J_0(kr) dk$ with maximum at $(r=0,\ z=L/2)$,

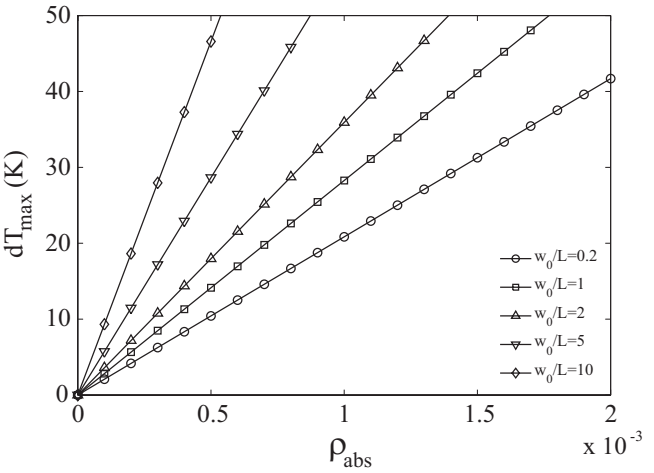

FIG. 10. Maximum elevation temperature as a function of ρ_{abs} for different values of w_0/L.

$$dT_{\max} = \int_0^\infty k\tilde{T}(k,L/2) dk. \tag{22}$$

Figure 9(b) shows the dependence of the absorption ρ_{abs} versus input power ρ that corresponds to static reorientation diagrams. The maximum temperature elevation $dT_{\max}$ is presented in Fig. 10 as a function of ρ_{abs} for different values of w_0/L, taking $\kappa_{\mathrm{LC}}=2$ mW/(K cm) [52]. We conclude that it is preferable to use a small beam waist in order to minimize the liquid-crystal heating. Noting that common nematic liquid crystal may have a temperature range of existence of several tens of degrees, one could foresee the possible use of dye-doped NLC defect layers in 1D periodic photonic structures.

The case of pure NLC can be referenced on the basis of these results. Indeed, the linear absorption coefficient is $\alpha^{(\mathrm{pure})} \sim 0.05\ \mathrm{cm}^{-1}$ in that case, leading typically to a 10^3 lower absorbed intensity. Therefore, moderate elevation temperature is expected in that case even if high values of ρ are used.

Finally, it is worth mentioning that, despite the fact that the exact resolution of the dynamical heating problem has no analytical simple formulation, the problem is well-posed using both the Hankel and Laplace transforms in the framework of the present model. However, its resolution is beyond the scope of the present study. Nevertheless, one can expect that resonant absorption induces temperature elevation that may lead to nematic-isotropic phase transition of the liquid crystal, thus making the whole approach presented here inapplicable in a realistic situation. This makes pure NLCs more attractive for the realization of all-optical switching photonics devices.

IV. CONCLUSIONS

We have performed a comparative study of the light-induced Fréedericksz transition for linearly polarized light in one-dimensional dielectric periodic structures with pure and without dye-doped nematic liquid crystal defect layers. The optical Fréedericksz transition threshold is spectrally modulated in both cases and the order of the transition can be

either first-or second-order depending on the sign of the detuning between the pumping light and the nearest defect mode frequencies. A positive detuning is associated with a positive feedback mechanism for the optical torque that leads to first-order transition, while it is not the case for negative detuning where transition is second-order. In contrast to the case of simple nematic liquid crystal films, the presence of dye dopant known to enhance the optical torque does not lead to a systematic lowering of the optical reorientation threshold. Indeed, the resonant absorption at defect mode frequencies competes with the dye-enhanced optical torque and may lead to an overall increase of the threshold if the defect mode is sufficiently localized. Both statics and dynamics of above-threshold orientational effects have been discussed. The stationary reorientation diagrams show a multistable behavior independent of the defect nature and detuning sign. In addition, switching dynamics exhibits transmission spikes whose linewidth can be several orders of magnitude lower than the characteristic orientational time of the liquid crystal material. Such ultrafast optical responses are attributed to the conjunction of high-quality defect modes together with a strong coupling between the liquid crystal and light propagating through the structure. However, in contrast to the pure case, these dynamical resonances are strongly damped in the dye-doped situation due to resonant absorption. Finally, thermal effects have been estimated and seem to restrict the use of dye-doped nematic liquid crystal defects.

ACKNOWLEDGMENTS

The work has been supported by the Australian Research Council through the Discovery and Centre of Excellence projects, and by the Coopération France-Australie project 21337.

[1] J. D. Joannopoulos, R. D. Meade, and J. N. Winn, *Photonic Crystals: Molding the Flow of Light* (Princeton University Press, Princeton, NJ, 1995).
[2] J. D. Joannopoulos, P. R. Villeneuve, and S. Fan, Nature **386**, 143 (1997).
[3] S.-Y. Lin, E. Chow, V. Hietala, P. R. Villeneuve, and J. D. Joannopoulos, Science **282**, 274 (1998).
[4] E. Moreno, L. Martín-Moreno, and F. Garcia-Vidal, Photonics Nanostruct. Fundam. Appl. **2**, 97 (2004).
[5] P. Rakich, M. Dahlem, S. Tandon, M. Ibanescu, M. Soljacic, G. Petrich J. Joannopoulos, L. Kolodziejski, and E. Ippen, Nature Mater. **5**, 93 (2006).
[6] S.-Y. Lin, V. M. Hietala, L. Wang, and E. D. Jones, Opt. Lett. **21**, 1771 (1996).
[7] K. Busch and S. John, Phys. Rev. Lett. **83**, 967 (1999).
[8] K. Yoshino, Y. Shimoda, Y. Kawagishi, K. Nakayama, and M. Ozaki, Appl. Phys. Lett. **75**, 932 (1999).
[9] K. Yoshino, S. Satoh, Y. Shimoda, Y. Kawagishi, K. Nakayama, and M. Ozaki, Jpn. J. Appl. Phys., Part 2 **38**, L961 (1999).
[10] E. Graugnard, J. S. King, S. Jain, C. J. Summers, Y. Zhang-Williams, and I. C. Khoo, Phys. Rev. B **72**, 233105 (2005).
[11] N. V. Tabiryan, A. V. Sukhov, and B. Y. Zel'dovich, Mol. Cryst. Liq. Cryst. **136**, 1 (1986).
[12] S. D. Durbin, S. M. Arakelian, and Y. R. Shen, Phys. Rev. Lett. **47**, 1411 (1981).
[13] B. Y. Zel'dovich, N. V. Tabiryan, and Y. S. Chilingaryan, Sov. Phys. JETP **54**, 32 (1981).
[14] B. Y. Zel'dovich and N. V. Tabiryan, Sov. Phys. JETP **55**, 656 (1982).
[15] H. L. Ong, Phys. Rev. A **28**, 2393 (1983).
[16] V. Fréedericksz and V. Zolina, Trans. Faraday Soc. **29**, 919 (1933).
[17] E. Santamato, B. Daino, M. Romagnoli, M. Settembre, and Y. R. Shen, Phys. Rev. Lett. **57**, 2423 (1986).
[18] E. Brasselet and L. J. Dube, Phys. Rev. E **73**, 021704 (2006).
[19] A. Vella, A. Setaro, B. Piccirillo, and E. Santamato, Phys. Rev. E **67**, 051704 (2003).
[20] C. Conti, M. Peccianti, and G. Assanto, Phys. Rev. Lett. **92**, 113902 (2004).
[21] M. Peccianti, C. Conti, G. Assanto, A. De Luca, and C. Umeton, Nature **432**, 733 (2004).
[22] A. Alberucci, M. Peccianti, G. Assanto, A. Dyadyusha, and M. Kaczmarek, Phys. Rev. Lett. **97**, 153903 (2006).
[23] M. Peccianti, A. Dyadyusha, M. Kaczmarek, and G. Assanto, Nat. Phys. **2**, 737 (2006).
[24] T. T. Alkeskjold, J. Laegsgaard, A. Bjarklev, D. S. Hermann, Anawati, J. Broeng, J. Li, and S.-T. Wu, Opt. Express **12**, 5857 (2004).
[25] J. Tuominen, H. J. Hoffrén, and H. Ludvigsen, J. Eur. Opt. Soc. Rapid Publ. **2**, 07016 (2007).
[26] H. Yoshida, C. H. Lee, Y. Miura, A. Fujii, and M. Ozaki, Appl. Phys. Lett. **90**, 071107 (2007).
[27] B. Maune, J. Witzens, T. Baehr-Jones, M. Kolodrubetz, H. Atwater, A. Scherer, R. Hagen, and Y. Qiu, Opt. Express **13**, 4699 (2005).
[28] P. El-Kallassi, R. Ferrini, L. Zuppiroli, N. Le Thomas, R. Houdré, A. Berrier, S. Anand, and A. Talneau, J. Opt. Soc. Am. B **24**, 2165 (2007).
[29] A. E. Miroshnichenko, I. Pinkevych, and Y. S. Kivshar, Opt. Express **14**, 2839 (2006).
[30] A. E. Miroshnichenko, E. Brasselet, and Y. S. Kivshar, Appl. Phys. Lett. **92**, 253306 (2008).
[31] I. Janossy and A. D. Lloyd, Mol. Cryst. Liq. Cryst. **203**, 77 (1991).
[32] E. Brasselet, T. V. Galstian, L. J. Dubé, D. O. Krimer, and L. Kramer, J. Opt. Soc. Am. B **22**, 1671 (2005).
[33] D. O. Krimer, L. Kramer, E. Brasselet, T. V. Galstian, and L. J. Dubé, J. Opt. Soc. Am. B **22**, 1681 (2005).
[34] E. Brasselet, B. Doyon, T. V. Galstian, and L. J. Dubé, Phys. Rev. E **67**, 031706 (2003).
[35] L. Marrucci, P. Maddalena, G. Arnone, L. Sirleto, and E. Santamato, Phys. Rev. E **57**, 3033 (1998).
[36] D. O. Krimer, G. Demeter, and L. Kramer, Phys. Rev. E **66**,

031707 (2002).
[37] I. Jánossy and T. Kósa, Opt. Lett. **17**, 1183 (1992).
[38] I. Jánossy, A. D. Lloyd, and B. S. Wherrett, Mol. Cryst. Liq. Cryst. **179**, 1 (1990).
[39] I. Jánossy and T. Kósa, Mol. Cryst. Liq. Cryst. **207**, 189 (1991).
[40] In the calculations, this formally corresponds to multiply the optical free energy given by Eq. (3) by the factor $[\mathrm{Re}(\epsilon_a) + \eta]/\mathrm{Re}(\epsilon_a)$, noting, however, that there is no dye-related free-energy density.
[41] D. W. Berreman, J. Opt. Soc. Am. **62**, 502 (1972).
[42] W. H. Press, S. A. Teukolsky, W. T. Vetterling, and B. P. Flannery, *Numerical Recipes: The Art of Scientific Computing* (Cambridge University Press, Cambridge, UK, 2007).
[43] K. Yoshino, Y. Ohmori, A. Fujii, and M. Ozaki, Jpn. J. Appl. Phys., Part 1 **46**, 5655 (2007).
[44] R. Ozaki, H. Moritake, K. Yoshino, and M. Ozaki, J. Appl. Phys. **101**, 033503 (2007).
[45] R. Ozaki, T. Matsui, M. Ozaki, and K. Yoshino, Appl. Phys. Lett. **82**, 3593 (2003).
[46] R. Ozaki, T. Matsui, M. Ozaki, and K. Yoshin, Jpn. J. Appl. Phys., Part 2 **41**, L1482 (2002).
[47] R. Ozaki, M. Ozaki, and K. Yoshino, Jpn. J. Appl. Phys., Part 2 **42**, L669 (2003).
[48] L. Marrucci, D. Paparo, P. Maddalena, E. Massera, E. Prudnikova, and E. Santamato, J. Chem. Phys. **107**, 9783 (1997).
[49] T. Kósa and I. Jánossy, Opt. Lett. **20**, 1230 (1995).
[50] M. Lax, J. Appl. Phys. **48**, 3919 (1977).
[51] E. Brasselet, A. Lherbier, and L. J. Dubé, J. Opt. Soc. Am. B **23**, 36 (2006).
[52] H. Ono and K. Shibata, J. Phys. D **33**, L137 (2000).